RSC Advances

PAPER

View Article Online
View Journal | View Issue

Cite this: *RSC Adv.*, 2014, **4**, 51884

Rayleigh-instability-driven morphology transformation of electrospun polymer fibers imaged by *in situ* optical microscopy and stimulated Raman scattering microscopy†

Ting-Hsien Lee, Yu-Jing Chiu, Yu-Cheng Lai, Ping-Wen Fan, Tyng-Yow Kuo, Ian Liau* and Jiun-Tai Chen*

Received 25th June 2014
Accepted 3rd October 2014

DOI: 10.1039/c4ra06228k

www.rsc.org/advances

Electrospinning is one of the most common methods to prepare polymer fibers with sizes ranging from several nanometers to hundreds of micrometers. In most studies of electrospun polymer fibers, the properties and morphologies of polymer fibers are controlled by changing the electrospinning conditions. Few studies focus on the post-treatments of polymer fibers, which are critical for many fiber-based applications. In this work, we investigate the morphology transformation of electrospun polystyrene (PS) fibers annealed on top of poly(methyl methacrylate) (PMMA) film-coated glass substrates. *In situ* optical microscopy and stimulated Raman scattering (SRS) microscopy are used to observe the transformation process, which is driven by the Rayleigh instability, the surface tensions, and the interfacial tensions of polymers. Depending on the thickness of the underlying PMMA films, the electrospun PS fibers may transform into hemispheres or disks. The growth rates of the undulating amplitude are also affected by the film thickness.

Introduction

In recent years, the electrospinning technique has been widely used to prepare polymer fibers with diameters ranging from nanometer to micrometer scales.[1,2] Electrospun fibers can be applied to different areas such as drug delivery,[3] tissue engineering,[4] wound dressings,[5] filtration,[6] and sensors.[7] The sizes and surface morphologies of the electrospun fibers need to be effectively controlled for different application purposes. To manipulate the morphologies and the properties of the electrospun fibers, the commonly used approach is by changing the experimental parameters in the electrospinning process. These parameters include the type of polymer, the polymer molecular weight, the solution concentration, the type of solvent, the flow rate, the working voltage, the working temperature, and the working distance.[1,8–10] The effect of post-treatment on the surface morphologies and properties of the electrospun fibers, however, is rarely studied.

Different post-treatment techniques have been applied to modify or improve the properties and morphologies of polymer films and polymer blends. Two of the most commonly used post-treatment techniques are thermal annealing and solvent annealing.[11,12] During the annealing processes, polymer chains become mobile and are capable of attaining a thermodynamic equilibrium. For the effect of post-treatment on the morphologies and properties of electrospun fibers, some studies have been conducted. For instance, Lim *et al.* studied the effect of thermal annealing on the morphologies of poly(L-lactic acid) (PLLA) nanofibers.[13] They found that the interfibrillar bonding of the PLLA nanofibers was enhanced after annealing. The Young's modulus of the fibers also increased because of the change in morphology and the increase in the crystallinity by thermal annealing. Liu *et al.* also investigated the effect of thermal annealing on the properties of electrospun nylon-6 fibers.[14] They observed that the metastable γ crystals melted and recrystallized into thermodynamically stable α-form crystals after thermal annealing. Despites these studies, the effects of many factors on the morphology and property changes of electrospun polymer fibers are still unclear. Therefore, further investigations are required.

Previously, we studied the morphology transformation by thermally annealing electrospun poly(methyl methacrylate) (PMMA) fibers in ethylene glycol.[15] Ethylene glycol is a non-solvent for PMMA and provides a uniform environment for thermal annealing.[16,17] Because of the surface tension between PMMA and ethylene glycol, the surfaces of the PMMA fibers undulate and break into polymer spheres. The main interface to be concerned is the interface between the polymer and ethylene glycol, and the substrate effect can be eliminated.[15]

Department of Applied Chemistry, National Chiao Tung University, Hsinchu, 30010, Taiwan. E-mail: ianliau@mail.nctu.edu.tw; jtchen@mail.nctu.edu.tw

† Electronic supplementary information (ESI) available: Raman spectra of PS and PMMA. See DOI: 10.1039/c4ra06228k

To understand the substrate effect on the morphology transformation of polymer fibers upon thermal annealing, we also studied the morphology transformation of electrospun polystyrene (PS) fibers annealed on PMMA-coated glass substrates.[18] Compared with the uniform environment in ethylene glycol, the morphology transformation of the PS fibers was observed to be significantly affected by the underlying substrates.

In order to understand the transformation process of electrospun fibers upon annealing further, here we anneal PS fibers (average fiber diameter ~4.62 μm) on PMMA films with different thicknesses and employ *in situ* optical microscopy to observe directly the morphology transformation and the intermediate morphologies (undulated structures). When PS fibers are annealed on a PMMA film with a thicker thickness (~26 μm), the PS fibers transform into hemispheres embedded in the upper part of the PMMA film, driven by the reduction of the interfacial energy between PS and PMMA. By comparison, when PS fibers are annealed on a PMMA film with a thinner thickness (~4 μm), the PS fibers transform into disks embedded in the PMMA matrix. For a thinner PMMA film, the transformation process of the PS fiber is affected by the underlying glass substrate. The growth rate of the undulated amplitude is also observed to be affected by the thickness of the PMMA film, due to the interactions between the polymers and the glass substrates. These deductions are supported with observations made after removing PS or PMMA selectively using hexane or acetic acid, respectively. The removing process may, however, cause distortions and affect the morphologies of the PS/PMMA composites. In order to eliminate these concerns, we particularly employ stimulated Raman scattering (SRS) microscopy.

SRS microscopy was first developed by Xie *et al.* and has become a powerful tool for nondestructive, chemically specific, and video-rate imaging without labeling.[19] To produce SRS signals, two laserbeams (termed the "pump" and the "Stokes" beams) at frequencies ω_p and ω_S are normally used as excitation. When the beat frequency of the two optical fields ($\Delta\omega = \omega_p - \omega_S$) is equal to the frequency of a Raman-active molecular vibration of the substance under illumination, there is a gain (a loss) in the intensity of the Stokes (the pump) beams as a result of the stimulated transition. Distinct from coherent anti-Stokes Raman scattering (CARS) microscopy, another modality of chemical imaging, SRS microscopy does not have nonresonant background. More importantly, the intensity of SRS is linearly proportional to the quantity of molecular vibrations in resonant, thereby making possible quantification of a sample. Similar to other modalities of multiphoton imaging such as two-photon excited fluorescence microscopy, SRS microscopy allows three-dimensional (3D) imaging of thick samples. These unique features renders SRS microscopy an ideal tool to visualize selectively the 3D morphological transformation of individual components of a composite material. Until now, SRS microscopy is mainly utilized to image biological systems. Applications of SRS microscopy to investigate polymeric composite materials are rare.

The morphology transformation of the electrospun PS fibers is related to the Rayleigh instability and the surface tensions of the polymers.[20–22] The Rayleigh instability is commonly seen in daily life. In 1873, Joseph Plateau first studied the instability of liquid cylinders.[23] He found that the surface of an infinite long liquid cylinder can undulate. When the wavelength (λ) of the undulation is larger than the perimeter ($2\pi R_0$) of the liquid cylinder, the cylinder breaks into a chain of drops.[24] This phenomenon is later investigated by Lord Rayleigh, who proved that the undulation wavelength is determined by the fastest distortion mode.[25]

Nichols and Mullins later applied the Rayleigh's theory to solid cylinder using similar calculations.[26] They studied the mass transport of solid cylinders and found first-order perturbation solutions based on surface diffusion and volume diffusion. For a long cylinder with a radius of R_0, an infinitesimal longitudinal sinusoidal perturbation is considered. The undulated surface can be described by the following equation

$$R = R_0 + \delta \sin(2\pi/\lambda)z \quad (1)$$

where λ is the undulation wavelength, δ is the undulation amplitude, and z is the main coordinate along the cylinder.[27] Considering the surface diffusion, which dominates in most situations, the perturbation with the wavelength greater than $\lambda_0 = 2\pi R_0$ is unstable, and its amplitude can increase spontaneously with time. The maximum growth rate of the perturbation amplitude occurs for the perturbation with the wavelength $\lambda_m = 2\pi\sqrt{2}R_0 = 8.89\ R_0$.[26] With the assumption of the volume conservation, the cylinder breaks up into spheres with an average diameter $d = 3.78\ R_0$.

In this work, we investigate the transformation processes of the electrospun PS fibers driven by the Rayleigh instability, the surface tensions, and the interfacial tensions of polymers. When electrospun polymer fibers are annealed on substrates, the situation is more complicated than the original Rayleigh instability. More interfaces including the polymer/air, polymer/polymer, polymer/substrate, and air/substrate interfaces need to be considered. The driving force for the morphology transformation is the reduction of the interfacial energies between PS and PMMA, as well as the surface energies of the polymers.

Experimental section

Materials

Poly(methyl methacrylate) (PMMA) and polystyrene (PS) were obtained from Sigma Aldrich with weight average molecular weights (M_w) of 75 and 192 kg mol^{-1}, respectively. Dimethylformamide (DMF), tetrahydrofuran (THF), cyclohexane, and acetic acid were purchased from Tedia. The glass substrates were obtained from the FEA company.

Preparation of electrospun PS fibers

To prepare the electrospun PS fibers, a PS solution (30 wt% in DMF) was added to a syringe. The syringe was attached to a capillary nozzle (inner diameter: 0.41 mm), which was connected to a high-voltage power supply (SIMCO) with a voltage range of 10–30 kV. The electrospinning process was performed in a vertical spinning configuration at room temperature.

The flow rate of the polymer solution was controlled by a syringe pump (KD Scientific) at 1 mL h^{-1}. The working distance between the capillary nozzle and the grounded collector was set at 10 cm. Under these conditions, the average diameter of the electrospun PS fibers is ~4.62 μm.

Thermal annealing process of electrospun PS fibers on different substrates

After the fabrication of the electrospun PS fibers, the fibers were collected and placed on different substrates. To prepare the glass substrates coated with PMMA films of different thicknesses, PMMA solutions (20 or 25 wt% in THF) and a metal blade with different gaps were used by applying the blade coating technique. After the evaporation of the solvent, PMMA films with thicknesses from 3 to 26 μm can be obtained.

The PS fibers were then placed on glass-only or PMMA film-coated glass substrates. A heating stage (FP82, Mettler) equipped with an optical microscope was used to thermally anneal the samples. The initial annealing temperature, the temperature increasing rate, and the annealing time were controlled by a temperature controller. For most annealing experiments, the annealing temperatures were fixed at ~240 °C, and the morphology transformation of the PS fibers can be *in situ* observed by the optical microscope. For the selective removal process, cyclohexane and acetic acid are chosen as the solvents to remove PS and PMMA, respectively.

Structure analysis and characterization

The glass transition temperatures (T_g) of PMMA and PS were measured by the differential scanning calorimetry (DSC) (EXSTAR 6000, Seiko Instruments). During the annealing process, the annealing time and temperature were controlled by a temperature controller (FP90, Mettler). The structure transformation of the electrospun PS fibers by thermal annealing was observed by an optical microscope (Axiophot, Zeiss) under condenser lens (10×) and projector lens (40×). The *in situ* images and movies from the optical microscope (OM) were acquired by an imaging software (upmost). A scanning electron microscope (SEM) (JSM-7401F, JEOL) at an acceleration voltage of 10 kV was also used to examine the morphologies of the polymer samples. Before performing SEM, the samples were dried by a dessicator and coated with platinum (~4 nm).

The SRS system was modified from a setup described before.[28,29] In brief, a mode-locked Nd : Vanadate laser (picoTrain, High-Q laser; 1064 nm, 7 ps, 76 MHz) and a synchronously pumped, frequency-doubled optical parametric oscillator (OPO, Levante, APE; tunable between 775 to 975 nm) served as the Stokes and the pump beams. To image selectively the PS domain of the composite, the wavelength of the OPO was adjusted such that the beating frequency of the pump and Stokes beams matched the resonance frequency (3054 cm^{-1}; Fig. S1 in ESI†) of the C–H stretching mode of the benzene moiety of PS, a distinct vibration mode abundant in PS but not in PMMA. To extract the SRS signal, we employed phase sensitive detection. We modulated the Stokes beam at approximately 10 MHz with an electro-optical modulator (M360-80, ConOptics) and demodulated with a lock-in amplifier (SR-844, Stanford Research Systems). To generate an SRS image, the demodulated signal, which was detected with a photodiode (818-BB-40, Newport), was recorded while the sample was scanned relative to the laser focus using a piezo-stage (P-563.3CD, Physik Instrument).

Results and discussion

In this work, we investigate the substrate effect on the transformation of electrospun polymer fibers upon thermal annealing. Fig. 1 shows the schematics illustration of the electrospinning setup and the annealing process of PS fibers on glass and PMMA film-coated substrates. At first, electrospun fibers are prepared by the electrospinning technique. After the electrospun PS fibers are collected, they are annealed at 240 °C on different substrates. Three different types of substrates are used in this work. The first type of substrate is a bare glass substrate. The second and the third types of substrates are glass substrates coated with thicker (thickness ~26 μm) and thinner (thickness ~4 μm) PMMA films, respectively. Depending on the substrates, the PS fibers can transform into different morphologies. When PS fibers are annealed on a bare glass substrate, wetting of the polymer fibers occurs because of the high surface energy of the glass substrate. When the PS fibers are annealed on PMMA film-coated glass substrates, the PS fibers transform into polymer hemispheres or disks, driven by the Rayleigh instability and the lower surface tension of PS.

First, we prepare the PS fibers by electrospinning. Dimethylformamide (DMF) is chosen as the solvent to dissolve PS, because it has a high boiling point (152–154 °C), a high dipole moment (3.82 Debye), and a high dielectric constant (37 at 20 °C), allowing a better charge induction ability for polymer solution in an electric filed.[30] Fig. 2 shows the SEM images of electrospun PS fibers using different electrospinning conditions. One of the common ways to change the sizes and morphologies of the electrospun polymer fibers is by varying the polymer concentration because the solution viscosity is higher at a higher polymer concentration.[31,32] Fig. 2a–c shows the SEM images of PS (M_w: 192 kg mol^{-1}) fibers prepared using different PS concentrations (20, 25, and 30 wt%), while keeping other electrospinning parameters constant (voltage: 10 kV, working

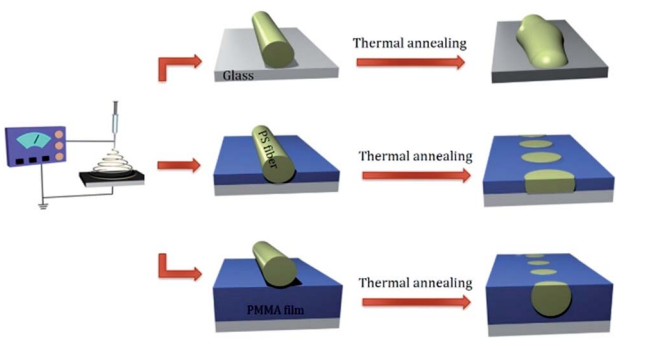

Fig. 1 Schematic illustration of the electrospinning setup and the annealing processes of electrospun PS fibers on different substrates.

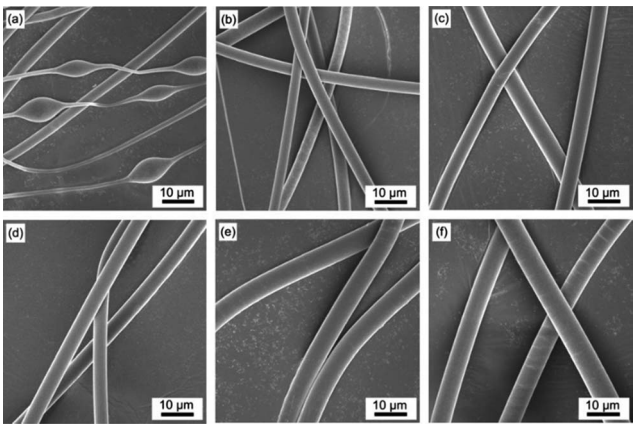

Fig. 2 SEM images of electrospun PS (M_w: 192k) fibers prepared by different conditions. The voltage and the working distance are 10 kV and 10 cm, respectively. (a–c) PS in DMF with a flow rate of 1 mL h^{-1} at different concentrations: (a) 20, (b) 25, and (c) 30 wt%. (d–f) 30 wt% PS in DMF at different flow rates: (d) 1, (e) 3, and (f) 5 mL h^{-1}.

distance: 10 cm, and flow rate: 1 mL h^{-1}). If the polymer concentration is low, the viscosity of the polymer solution may not be enough. After the solution is ejected to the electric field, the jet is affected by the whipping instability and the stable jet cannot be formed. Therefore, defected beaded polymer fibers can be easily obtained. As shown in Fig. 2a, the beaded structure can be observed by using a 20 wt% of PS solution. With a higher polymer concentration, more polymer entanglements are involved, and a stable jet can be formed. It has been shown that the diameter of the polymer fiber increases with the polymer concentration according to a power law relationship.[33] As shown in Fig. 2b–c, the diameters of the electrospun PS fibers increase from ~3–4 μm for 25 wt% to ~4–5 μm for 30 wt%. The diameters of the electrospun fibers can become even larger with higher polymer concentrations. But the high solution viscosity may increase the difficulty to eject the solution from the capillary nozzle.[34]

Not only the polymer concentration, the fiber diameter can also be controlled by changing the flow rate. As the flow rate increases, the fiber diameter of the electrospun fibers also increases and more polymer fibers are generated. Fig. 2d–f are the SEM images of electrospun PS (M_w: 192 kg mol^{-1}) fibers prepared using different flow rates (1, 3, and 5 mL h^{-1}) while keeping other electrospinning parameters constant (voltage: 10 kV, working distance: 10 cm, and polymer concentration: 30 wt%). We can see that the fiber diameter increases with the flow rate. The diameters of the electrospun PS fibers are found to increase from ~4 μm for 1 mL h^{-1} to ~8 μm for 5 mL h^{-1}.

After the fabrication of the electrospun PS fibers, they are annealed on different substrates. When the polymer chains are annealed at a temperature higher than its glass transition temperature, the polymer chains are mobile and can achieve their equilibrium morphologies. After annealing, the wetting behavior of the fibers on the substrates depends on the spreading coefficient (S), given by

$$S = \gamma_{SG} - \gamma_{SL} - \gamma \quad (2)$$

where γ_{SG}, γ_{SL}, and γ are the interfacial tensions of solid–gas, solid–liquid, and liquid–gas, respectively. If the value of S is positive, total wetting occurs and the substrate is covered by a polymer wetting layer. If the value of S is negative, partial wetting occurs and the polymer melt wets the substrate with a contact angle θ, defined by the Young's equation: $\theta = \cos^{-1}((\gamma_{SG} - \gamma_{SL})/\gamma)$. For partial wetting, the liquid is referred to as "mostly non-wetting" if θ is larger than $\pi/2$ and as "mostly wetting" if θ is smaller than $\pi/2$.[35]

First, we study the fibers annealed on glass substrates. The surface tension of the glass substrate (54.9 dyne cm^{-1}) is higher than those of most polymer melts, and the surface tensions of the PS melts at 20 and 140 °C are 40.7 and 32.1 dyne cm^{-1}, respectively. Fig. 3 shows the OM results by annealing the electrospun PS fibers on glass substrates at 240 °C for different periods of time. We find that the wetting of the PS fibers on the glass substrate occurs in a shorter time when the fibers are annealed at higher annealing temperatures because of the lower polymer viscosity. It is noted that the PS fibers does not wet the glass substrate uniformly. This result is because that the electrospun fibers are not straight and are not in contact with the substrate uniformly.[15]

Then we study the structure transformation of electrospun PS fibers annealed on PMMA-coated substrates at 240 °C. The morphology transformation can be *in situ* observed by OM. Determined by the differential scanning calorimetry, the glass transition temperatures (T_g) of PMMA and PS are 105 and 107 °C, respectively. The annealing temperature (240 °C) is far above the T_g of PMMA and PS. Thus, both polymers are mobile during the annealing process. The instability of cylindrical PS

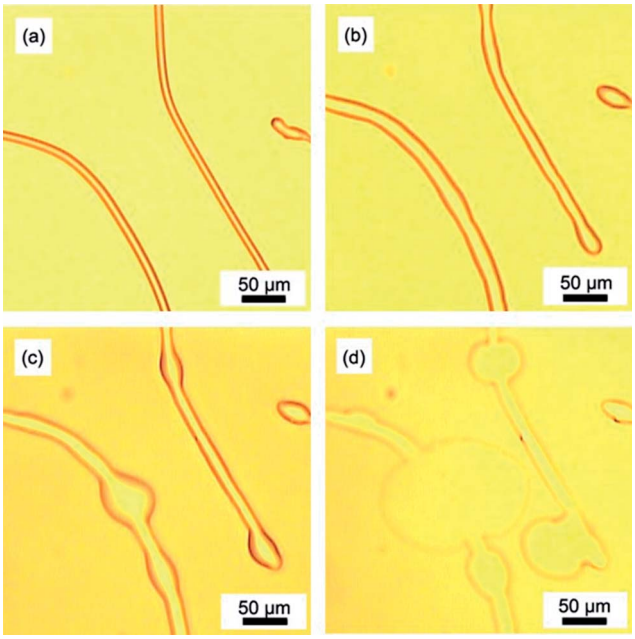

Fig. 3 OM images of PS fibers annealed at 240 °C on the glass substrates for different times: (a) 2, (b) 4, (c) 16, and (d) 36 min.

fibers and their transformation into a series of hemispheres can be induced by annealing. We prepare PMMA films with different thicknesses (4 and 26 μm), and the thickness effect of the PMMA film on the transformation process is also discussed in this work.

Fig. 4 shows the OM images of PS structures by annealing PS fibers on thicker PMMA films (thickness ~26 μm) at 240 °C for different periods of time. Different from the results obtained by annealing electrospun PS fibers on glass substrates, the presence of the PMMA film causes the electrospun PS fibers to undulate during the thermally annealing process and transform into a line of droplets. The driving force for the morphology transformation is the reduction of the interfacial energy between PS and PMMA, as well as the surface energies of the polymers. From the literature, the surface tensions of PS and PMMA are 40.7 and 41.1 dyne cm^{-1}, respectively. We propose our model of the morphology transformation by considering that the surface tension of PS is lower than that of PMMA. Under thermal annealing at 240 °C, both PS and PMMA are mobile. The electrospun PS fibers sink into the PMMA film to reduce the contact area between the polymer and air to decrease the surface energy. At the same time, the cylindrical fiber also undulates and transforms in order to decrease the interfacial area between PS and PMMA, similar to the classical Rayleigh instability. Finally, PS hemispheres are formed and embedded in the PMMA film. The time of the undulation state of the PS fiber is very short, but it can still be *in situ* observed in the OM images.

Not only on a PMMA film with a thicker thickness (~26 μm), but the PS fibers are annealed also on PMMA films with a thinner thickness. Fig. 5 shows the transformation of electrospun PS fibers into a series of PS hemispheres by annealing the fibers on a PMMA film of 4 μm at 240 °C. The transformation times from fibers to hemispheres are observed to be longer for PS fibers annealed on the thinner PMMA film. The slower kinetics at lower film thicknesses are due to the effect from the underlying glass substrates. For PS fibers annealed on a thicker PMMA film, the distance between the fiber and the substrate is larger and the effect of the underlying substrate is diminished. Later, we will discuss the effect of film thickness on the transformation kinetics of the fibers more quantitatively.

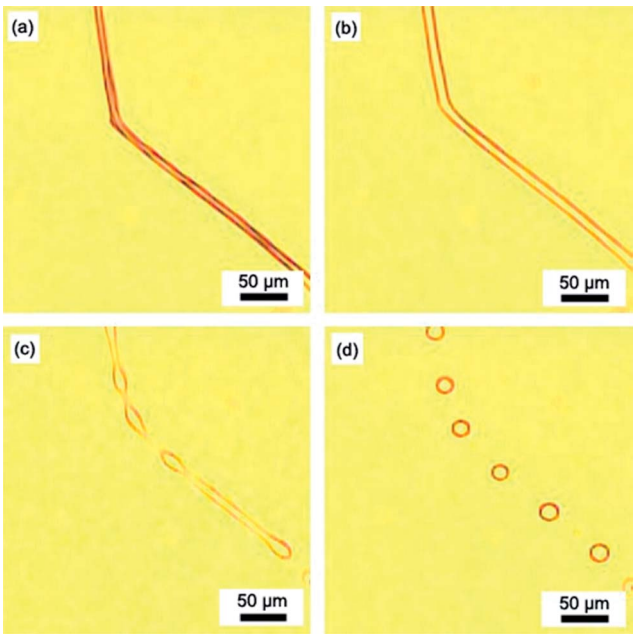

Fig. 4 OM images of electrospun PS fibers annealed at 240 °C on PMMA film-coated glass substrates for different times: (a) 50, (b) 90, (c) 140, and (d) 160 s. The thickness of the PMMA film is ~26 μm.

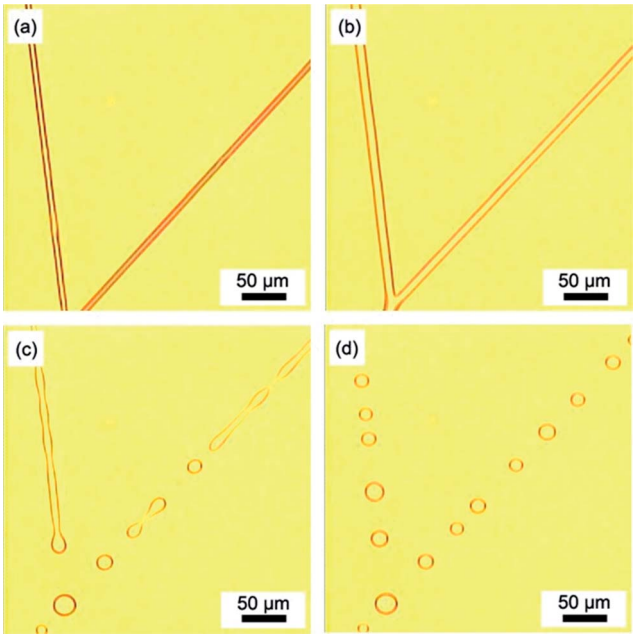

Fig. 5 OM images of electrospun PS fibers annealed at 240 °C on PMMA film-coated glass substrates for different times: (a) 70, (b) 110, (c) 200, and (d) 210 s. The thickness of the PMMA film is ~4 μm.

To further confirm the three-dimensional shape of the transformed PS particles and to understand the transformation mechanism, selective removal approaches are applied. PS or PMMA in the polymer composites are removed using selective solvents. Cyclohexane is a non-solvent for PMMA and can be used to remove the PMMA domain selectively. On the other hand, acetic acid is a non-solvent for PS and can be used to remove the PS domain selectively.

The selective removal procedures are performed for the samples with different PMMA film thicknesses. Fig. 6a shows the schematic illustration of the experimental process to remove the PMMA film or the PS particles selectively for the samples with the higher PMMA film thickness (~26 μm). Fig. 6b is the SEM image of the porous PMMA film after the PS particles are removed. The pore sizes in the PMMA film correspond to the sizes of the embedded PS particles. The SEM image of a PS hemisphere by removing the PMMA film is shown in Fig. 6c. The hemispherical shape of the PS particle can be observed. Some of the PMMA film is not dissolved by acetic acid completely, and irregular precipitates from the undissolved PMMA can also be seen, as shown in Fig. 6c.

The selective removal process is also performed for the samples with the thinner PMMA film thickness (~4 μm), as

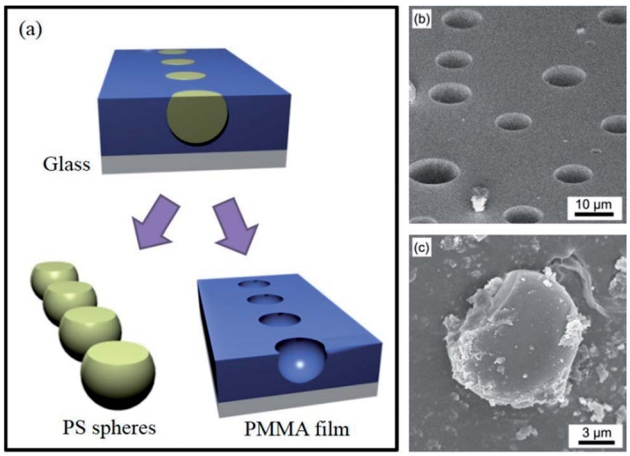

Fig. 6 (a) Schematic illustration of the experimental process to remove selectively the PMMA film or the PS particles. (b) SEM image of the PMMA film (thickness ~26 μm), in which PS particles are removed. (c) SEM image of a PS hemisphere.

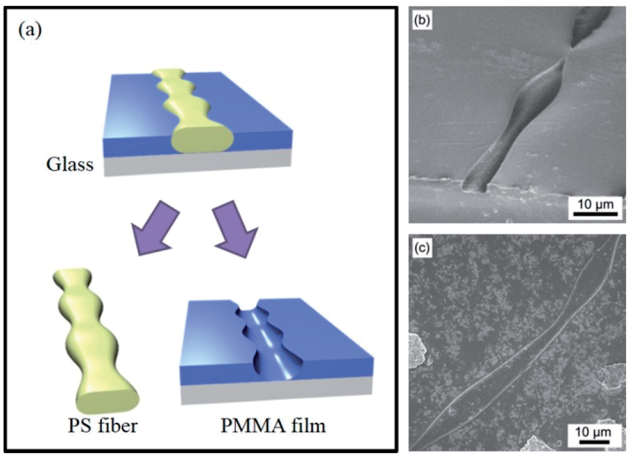

Fig. 8 (a) Schematic illustration of the experimental process to remove selectively the PMMA film or the PS structure. (b) SEM images of the PMMA film, in which the PS structure is removed. (c) SEM image of an undulated PS structure.

shown in Fig. 7. Since the PS fibers transform into disks after the annealing process in the case of thinner PMMA films, porous PMMA films with disk-shaped pores are formed after the PS disks are removed (Fig. 7b). The PS disks can also be revealed by removing the PMMA film selectively (Fig. 7c).

Based on our model, the transformation of the PS fibers into particles is achieved by first forming undulated structures. To prove this model, we try to anneal the samples at shorter times in order to observe the undulated structures. PMMA films with undulated channels are observed after the selective removal process, implying the formation of the undulated PS structures, as shown in Fig. 8b. The undulated PS structures are also revealed by removing the PMMA film selectively (Fig. 8c).

On the basis of the experimental results, the transformation processes of electrospun polymer fibers on films with different thickness are summarized in Fig. 9. When the samples are annealed at the temperatures higher than the glass transition temperatures of both PS and PMMA, the polymer chains have enough mobilities to achieve more stable morphologies. The PS fibers first sink into the PMMA films to reduce the interfacial area between the polymer composite films and air. Later, the PS fibers undulate and transform into hemispherical shape particles embedded in the PMMA film. The transformation process reduces the interfacial area between PS and PMMA, driven by the Rayleigh instability and the lower surface tension of PS. Therefore, the interfacial energy between PS and PMMA is decreased. By removing the PMMA film selectively, the hemispherical shape of the PS particles can be confirmed. The shapes of the transformed PS particles are also affected by the film thickness. The bottom parts of the PS particles are spherical when the PMMA film is thicker. On the other hand, the PS particles are in a disk shape when the PMMA film is thinner.

For the transformation process of electrospun fibers, we want to understand the effect of the underlying film thickness on two aspects. The first aspect is related to the transformation kinetics, such as the growth rate of the undulated amplitude, which is related to the viscoelastic properties of the materials

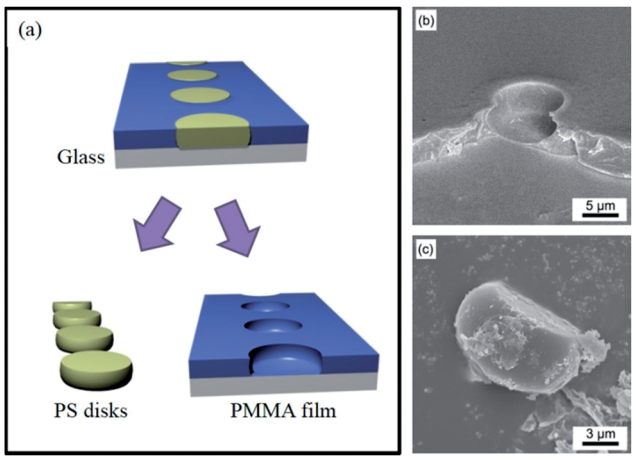

Fig. 7 (a) Schematic illustration of the experimental process to remove selectively the PMMA film or the PS particles. (b) SEM image of the PMMA film (thickness ~4 μm), in which PS particles are removed. (c) SEM image of a PS disk.

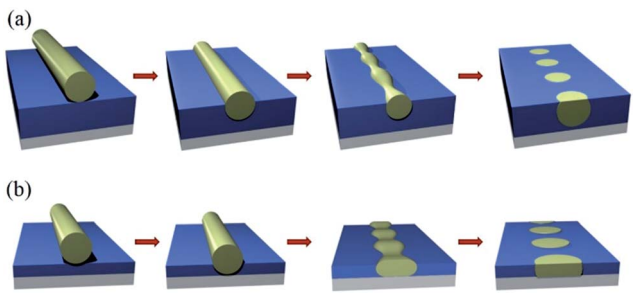

Fig. 9 Proposed models of the transformation processes of the electrospun PS fibers annealed at 240 °C on PMMA films with thick (a) and thin (b) thicknesses.

and may be affected by the glass substrate when the film thickness is too thin. The second aspect is related to the sizes of the transformed PS particles, which may be deviated from the theoretical values predicted by the Rayleigh instability.

First, we study the effect of film thickness on the transformation kinetics. Fig. 10a shows the OM images of electrospun PS fibers annealed on a PMMA film (thickness ~11 μm) at 240 °C for different periods of time. The growth rate of the undulated amplitude can be extracted from the size change of the electrospun fibers in the OM images. To perform the data extraction, we adopt the calculation method used by Elemans *et al.*, who investigated the interfacial tensions between two polymer materials applying the breaking thread method.[36]

At the beginning of the transformation process, the electrospun PS fibers are subjected to small sinusoidal perturbations and the total interfacial areas decrease with the increasing amplitude.[25] Therefore, the undulation wavelength (λ) must be larger than the original perimeter of the fibers. A dimensionless wave number (X) can be defined by the following equation

$$X = (2\pi R_0)/\lambda \quad (3)$$

where R_0 is the original radius of the electrospun fibers and λ is the undulation wavelength.[36] Thus, only perturbations with $X < 1$ can grow spontaneously.

During the transformation process, the amplitudes of perturbation (α) on the fibers grow exponentially with time

$$\alpha = \alpha_0 \, e^{qt} \quad (4)$$

where α_0 is the original amplitude and q is the growth rate of the undulated amplitude. The growth rate (q) is given by

$$q = (\sigma \, \Omega \, (\lambda, p))/(2\eta_c \, R_0) \quad (5)$$

where σ is the interfacial tension between the two polymers, η_d is the viscosity of the disperse (fiber) phase, η_c is the viscosity of the continuous (film) phase, p is the viscosity ratio between the two polymers, and Ω (λ, p) is a tabulated function.[36,37]

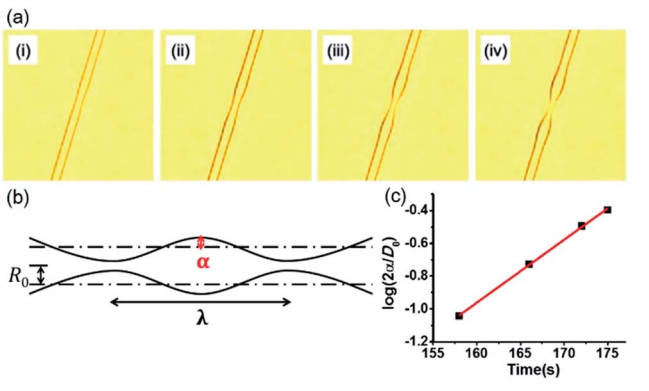

Fig. 10 (a) OM images of an electrospun PS fiber annealed at 240 °C on a PMMA film (thickness ~9.6 μm) for different times. (b) Illustration of an undulated fiber. (c) Plot of the log(2α/D_0) *versus* time where D_0 is the diameter of the fiber. The slope of the fitted line represents the growth rate of the undulated amplitude.

Therefore, the growth rate of the undulated amplitude is affected by the interfacial tensions and the viscosities of the polymers. An increase in the annealing temperature and a decrease in the molecular weights of the polymers are expected to increase the growth rate of the undulated amplitude.

An alternative analysis procedure that can be used to acquire the growth rate of the undulated amplitude (q) is by measuring the amplitude (α), as long as the perturbation remains sinusoidal. The amplitude (α) can be calculated by the following equation

$$\alpha = (b - a)/4 \quad (6)$$

where b is the thickest diameter and a is the thinnest diameter. The values of a and b at different annealing times can be directly measured from the OM images, and the values of α at different times can be calculated. Eqn (4) can be rewritten as the following

$$\log(2\alpha/D_0) = qt/\ln(10) \quad (7)$$

where D_0 is the diameter of the fiber, q is the growth rate of the undulated amplitude, and t is the annealing time. From the plot of log(2α/D_0) *versus* time, the growth rate of the undulated amplitude can be obtained from the slope (q = slope × ln(10) = slope × 2.303). For example, the plot of log(2α/D_0) *versus* time for annealing the PS fibers on a PMMA film with a thickness of ~9.6 μm is shown in Fig. 10c and the growth rate of the undulated amplitude is calculated to be 0.088 (s^{-1}).

We then compare the growth rates of the undulated amplitude at different film thicknesses. As shown in Fig. 11, the growth rates are ~0.1 (s^{-1}) when the thicknesses are larger than ~10 μm. When the thicknesses are thinner, the growth rates decrease and reach ~0.03–0.04 (s^{-1}) for thicknesses lower than ~8 μm. The slower kinetics at lower film thicknesses are because of the effect from the underlying glass substrates. Since the average diameter of the electrospun PS fiber is ~4.62 μm, the thickest undulated diameter predicted by Rayleigh instability is ~8.73 μm. Therefore, when the film thickness is less than ~8 μm, the undulated PS structures are closer to the underlying substrate and the growth rate of the undulated amplitude are reduced because of the interactions between the polymers and the glass substrates.

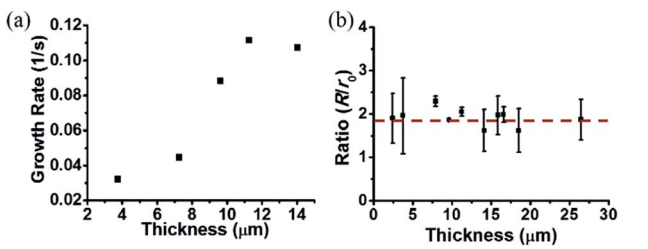

Fig. 11 (a) Plot of the growth rate of the undulated amplitude *versus* the thickness of the PMMA film. (b) Plot of the ratio of the radius of the spheres (R) to the radius of the fibers (r_0) *versus* the thickness of the PMMA film. The red line indicates the theoretical ratio (~1.89).

Then we discuss whether the values of the sizes of the transformed PS particles annealed on PMMA films of different thicknesses are deviated from the theoretical values predicted by the Rayleigh instability. According to the theory of the Rayleigh instability, the cylinder undulates with the maximum wavelength $\lambda_m = 8.89\ r_0$ when the instability occurs at the highest growth rate, where r_0 is the original radius of the liquid cylinder.[18] The radii of the transformed particles (R) are proportional to the radii of the original fibers (r_0) at a ratio of ~1.89. To obtain the ratios of the particle sizes to the original fiber radii at different PMMA film thicknesses, the sizes of the fibers and transformed spheres are individually measured. Fig. 11b shows the measured values of the ratios of the particle sizes to the original fiber radii at different film thicknesses, where the red line indicates the theoretical value of the ratio at ~1.89. We find that the measured values of the ratios agree well with the theoretical prediction at ~1.89, independent of the film thickness.

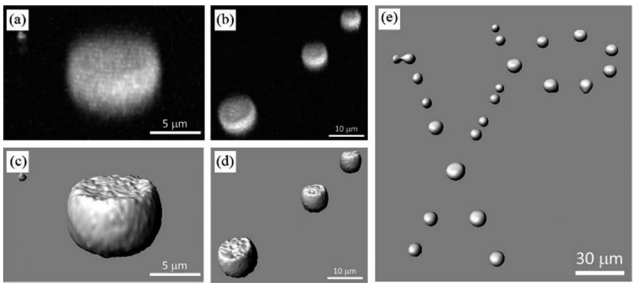

Fig. 12 SRS images of PS domains obtained from a PS/PMMA composite (thickness of the PMMA film ~26 μm) showing that the PS domains underwent a morphological transformation into hemispheres after annealing. (a and b) Raw data of one and three PS hemispheres. (c–e) Convolution data of one, three, and many PS hemispheres.

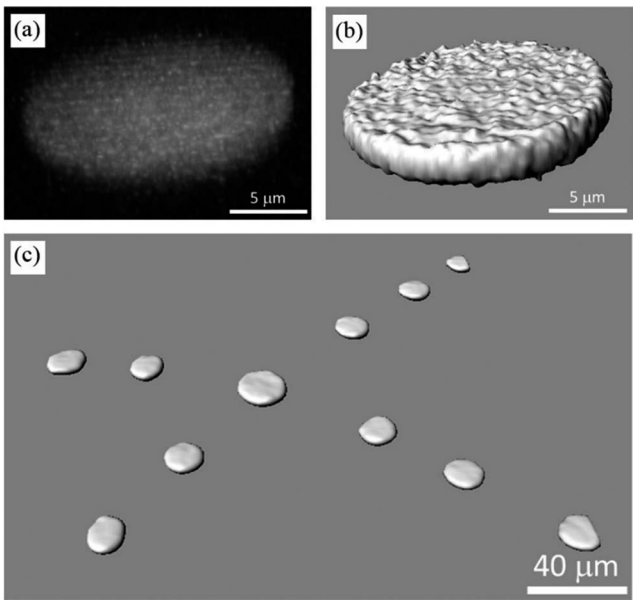

Fig. 13 SRS images of PS domains obtained from a PS/PMMA composite (thickness of the PMMA film ~4 μm) showing that the PS domains underwent a morphological transformation into disks after annealing. (a) Raw data of a PS disk. (b and c) Convolution data of one and many PS disks.

Although the transformed morphologies of the PS/PMMA composites can be characterized by the selective removal processes, as shown in Fig. 6–8, it is still highly desirable to study the morphologies of the composites when the two polymers are both present. To this end, we characterize the morphologies of the polymer composites with SRS microscopy.

Fig. 12 displays the SRS images of the PS domain obtained from PS fibers on PMMA films (thickness ~26 μm) after annealing. As shown from the result, hemispherical PS spheres are observed, which are in good agreement with the results from the selective removal processes. In contrast, for the samples by annealing the PS fibers on thinner PMMA films (thickness ~4 μm), the SRS microscopy is also performed. As shown from the result displayed in Fig. 13, the PS domains appear as disks, which also agree with our proposed model that the PS fibers transformed into PS disks when the PMMA film is thinner.

Our result represents a novel application of SRS microscopy on composite materials. Given the unique capability of SRS microscopy, we expect that this powerful tool will be applicable to other polymer systems and can shed light on fundamental problems in polymer science.

Conclusions

We study the morphology transformation of electrospun PS fibers on PMMA films with different thicknesses after thermal annealing. For PS fibers annealed on a PMMA film with a thicker thickness (~26 μm), the fibers transform into hemispheres embedded in the PMMA film, driven by the Rayleigh instability, the surface tensions, and the interfacial tension between PS and PMMA. For PS fibers annealed on a PMMA film with a thinner thickness (~4 μm), the fibers transform into disks embedded in the PMMA film. By using *in situ* optical microscopy and SRS microscopy, the transformation processes are observed and the quantitative analysis is performed. The sizes of the polymer particles agree well with the theoretical predictions, which are dependent on the initial fiber diameter and independent on the annealing temperature. The growth rate of the undulated amplitude decreases at thinner PMMA film thicknesses because of the interactions between the polymers and the glass substrates.

For the future work, we will study the transformation of hydrophobic polymer fibers annealed on hydrophilic polymer films instead of hydrophobic polymer films. In this way, hydrophilic polymer surfaces with spherical hydrophobic domains can be obtained, which will be useful for biomedical applications, such as protein patterning.

Acknowledgements

This work was supported by the Ministry of Science and Technology of the Republic of China.

Notes and references

1 Z. M. Huang, Y. Z. Zhang, M. Kotaki and S. Ramakrishna, *Compos. Sci. Technol.*, 2003, **63**, 2223–2253.
2 A. Greiner and J. H. Wendorff, *Angew. Chem., Int. Ed.*, 2007, **46**, 5670–5703.
3 N. Ashammakhi, I. Wimpenny, L. Nikkola and Y. Yang, *J. Biomed. Nanotechnol.*, 2009, **5**, 1–19.
4 Q. P. Pham, U. Sharma and A. G. Mikos, *Tissue Eng.*, 2006, **12**, 1197–1211.
5 M. Ignatova, N. Manolova and I. Rashkov, *Eur. Polym. J.*, 2007, **43**, 1609–1623.
6 X. H. Qin and S. Y. Wang, *J. Appl. Polym. Sci.*, 2006, **102**, 1285–1290.
7 R. Rojas and N. J. Pinto, *IEEE Sens. J.*, 2008, **8**, 951–953.
8 G. Taylor, *Proc. R. Soc. London, Ser. A*, 1969, **313**, 453–475.
9 C. Wang, C. H. Hsu and J. H. Lin, *Macromolecules*, 2006, **39**, 7662–7672.
10 P. Gupta, C. Elkins, T. E. Long and G. L. Wilkes, *Polymer*, 2005, **46**, 4799–4810.
11 I. M. Hodge, *Macromolecules*, 1987, **20**, 2897–2908.
12 Y. Kim, S. A. Choulis, J. Nelson, D. D. C. Bradley, S. Cook and J. R. Durrant, *Appl. Phys. Lett.*, 2005, **86**, 3.
13 E. P. S. Tan and C. T. Lim, *Nanotechnology*, 2006, **17**, 2649–2654.
14 Y. Liu, L. Cui, F. X. Guan, Y. Gao, N. E. Hedin, L. Zhu and H. Fong, *Macromolecules*, 2007, **40**, 6283–6290.
15 P. W. Fan, W. L. Chen, T. H. Lee and J. T. Chen, *Macromol. Rapid Commun.*, 2012, **33**, 343–349.
16 D. Chen, S. Park, J. T. Chen, E. Redston and T. P. Russell, *ACS Nano*, 2009, **3**, 2827–2833.
17 Y. C. Huang, P. W. Fan, C. W. Lee, C. W. Chu, C. C. Tsai and J. T. Chen, *ACS Appl. Mater. Interfaces*, 2013, **5**, 3134–3142.
18 P. W. Fan, W. L. Chen, T. H. Lee, Y. J. Chiu and J. T. Chen, *Macromolecules*, 2012, **45**, 5816–5822.
19 C. W. Freudiger, W. Min, B. G. Saar, S. Lu, G. R. Holtom, C. W. He, J. C. Tsai, J. X. Kang and X. S. Xie, *Science*, 2008, **322**, 1857–1861.
20 J. T. Chen, M. F. Zhang and T. P. Russell, *Nano Lett.*, 2007, **7**, 183–187.
21 D. Chen, J. T. Chen, E. Glogowski, T. Emrick and T. P. Russell, *Macromol. Rapid Commun.*, 2009, **30**, 377–383.
22 C. C. Tsai and J. T. Chen, *Langmuir*, 2014, **30**, 387–393.
23 J. Plateau, *Transl. Annu. Rep. Simthsonian Inst.*, 1873, 1863–1866.
24 P. G. de Gennes, F. Brochard-Wyart and D. Quere, *Capillarity and Wetting Phenomena*, Springer, New York, 2004.
25 L. Rayleigh, *Proc. London Math. Soc.*, 1878, **10**, 4–13.
26 F. A. Nichols and W. W. Mullins, *Trans. Metall. Soc. AIME*, 1965, **233**, 1840–1848.
27 S. Karim, M. E. Toimil-Molares, A. G. Balogh, W. Ensinger, T. W. Cornelius, E. U. Khan and R. Neumann, *Nanotechnology*, 2006, **17**, 5954–5959.
28 J. W. Jhan, W. T. Chang, H. C. Chen, Y. T. Lee, M. F. Wu, C. H. Chen and I. Laiu, *Opt. Express*, 2008, **16**, 16431–16441.
29 Y. M. Wu, H. C. Chen, W. T. Chang, J. W. Jhan, H. L. Lin and I. Liau, *Anal. Chem.*, 2009, **81**, 1496–1504.
30 L. Wannatong, A. Sirivat and P. Supaphol, *Polym. Int.*, 2004, **53**, 1851–1859.
31 J. T. Chen, W. L. Chen and P. W. Fan, *ACS Macro Lett.*, 2012, **1**, 41–46.
32 J. T. Chen, W. L. Chen, P. W. Fan and I. C. Yao, *Macromol. Rapid Commun.*, 2013, **35**, 360–366.
33 J. M. Deitzel, J. Kleinmeyer, D. Harris and N. C. B. Tan, *Polymer*, 2001, **42**, 261–272.
34 H. Fong, I. Chun and D. H. Reneker, *Polymer*, 1999, **40**, 4585–4592.
35 P. G. Degennes, *Rev. Mod. Phys.*, 1985, **57**, 827–863.
36 P. H. M. Elemans, J. M. H. Janssen and H. E. H. Meijer, *J. Rheol.*, 1990, **34**, 1311–1325.
37 S. Tomotika, *Proc. R. Soc. London, Ser. A*, 1935, **150**, 322–337.